Rheology of Water Flows Confined Between Multi-Layer Graphene Walls

F. Li,[1,a)] I. A. Korotkin,[1,2] and S. A. Karabasov[1]

[1]The School of Engineering and Materials Science, Queen Mary University of London, Mile End Road, E1 4NS London, United Kingdom

[2]Mathematical Sciences, University of Southampton, University Road, SO17 1BJ Southampton, United Kingdom

[a)] E-mail: f.li@qmul.ac.uk

KEYWORDS: nanoconfined water, transport properties, graphene layers, molecular dynamics

ABSTRACT: Water confined by hydrophilic materials shows unique transport properties compared to bulk water thereby offering new opportunities for development of nano-fluidic devices. Recent experimental and numerical studies showed that nano-confined water undergoes liquid-to-solid phase-like transitions depending on the degree of confinement. In the case of water confined by graphene layers, the Van der Waals forces are known to deform the graphene layers, whose bending leads to further non-uniform confinement effects. Despite the extensive studies of nano-confined water at equilibrium conditions, the interplay between the confinement and rheological water properties, such as viscosity, slip length and normal stress differences under

shear flow conditions, is poorly understood. The current investigation uses a validated all-atom non-equilibrium molecular dynamics model to simultaneously analyse continuum transport and atomistic structure properties of water in a slit between two moving graphene walls under Couette flow conditions. A range of different slit widths and velocity strain rates are considered. It is shown that under the sub-nanometer confinement, water loses its rotational symmetry of a Newtonian fluid. In such conditions, water transforms into ice, where the atomistic structure is completely insensitive to the applied shear force and which behaves like a frozen slab sliding between the graphene walls. This leads to the shear viscosity increase, although not as dramatic as the normal force increase that contributes to the increased friction force reported in previous experimental studies. On the other end of the spectra, for flows at large velocity strain rates in moderate to large slits between the graphene walls, water is in the liquid state and reveals a shear thinning behavior. In this case, water exhibits a constant slip length on the wall, which is typical of liquids in the vicinity of hydrophobic surfaces.

INTRODUCTION

Understanding of properties of water confined at the nanoscale is important for development of nano-fluidic devices[1-2]. Indeed, in comparison with bulk water, water confined by hydrophobic materials exhibits greatly enhanced transport properties which makes the design of nanoscale flow devices feasible[3-7]. Molecular Dynamics simulations[8-9] show that the enhanced water permeability property of nanofluidic devices is due to a reduced friction force between the water flow and solid walls. The friction force is inversely proportional to slip length and linearly depends on the shear viscosity.

The slip length characterises the effective repulsion of water molecules by a solid surface and is significantly increased in hydrophobic materials. For example, due to the water slip on their solid

interfaces, carbon nanotubes (CNT) generate flow rates which are several orders of magnitude larger in comparison with the flow rate predicted by the continuum theory based on the classical non-slip boundary condition[6]. For the same reason, the permeation rate of water flowing through graphene-based membranes can be $O(10^{10})$ times faster than the permeability of helium[7]. In general, hydrophobic materials are known to be characterized by an enhanced slippage as discussed by Vinogradova [10-11] and the references therein. In particular, for nano-confined water between graphene layers, existing experimental and computational data consistently predict a slip length that is much larger in comparison with the effective radius of Van der Waals forces (Table 1).

Table 1. Experimental results for slip length of nano-confined water in graphene

Reported by	Slip length (nm)
Ortiz-Young et al.[12]	12.5
Li et al.[13]	8
Maali et al.[14]	8

In comparison with the slip length, the role of water viscosity on the transport of water in hydrophobic materials such as CNT or graphene-based membranes[5-7] is not fully resolved. In the existing Atomic Force Microscopy experiments, the viscosity is measured *indirectly*, for example, by measuring the tangential force exerted on the AFM tip that is determined from a bending moment acted on the cantilever. Such measurements show a sharp increase of the shear force for sub-micron distances between the AFM needle and the substrate (Table 2). However, it remains unclear if, in addition to the shear force, the measured force also incorporates a large contribution of the normal force component. The force exerted in the normal direction to the tip surface in a nanometer-size gap can be very large when the distance between water atoms and the hydrophobic

surface becomes order of the effective radius of Van der Waals forces. In this case, the product of this force with the leading sine that contributes to the force component in the horizontal laboratory plane can be very significant (see further discussion in Supplementary Information III). Furthermore, the interactions between water atoms and the graphene surface under confinement also strongly depends on the density and temperature as well as molecular dipole moment orientation[15-18] on the solid surface.

Table 2. Experimental results for shear viscosity of nano-confined water in graphene

Reported by	Gap between tip and graphene (nm)	Confined shear viscosity/bulk shear viscosity
Ortiz-Young et al.[12]	0.7	2.5×10^4
Li et al.[19]	0.5	10^4
Li et al.[20]	≥ 2	1

The sensitivity of interaction between water atoms and a hydrophobic surface can be explained by properties of water phase transition from liquid-like to solid-like states [21-27] . Experimental and molecular dynamics studies revealed that crystals of 2D ice form in water at room temperature under a nanometer-size confinement[22]. For example, the freezing point of water in CNT experiments varies from -30ºC to 140ºC, when the carbon nanotube diameter changes from 1.05 nm to 1.52 nm[25]. Molecular Dynamics (MD) simulations showed that water changes its phase transition from discontinuous to continuous type when the tube diameter is smaller than 1.2 nm[28]. For water confined between graphene sheets, MD simulations showed that water undergoes a discontinuous phase transition above some critical density below which the phase transition becomes continuous[23]. Furthermore, MD simulations showed that the stacking pattern of solid-like water in nano-size gaps can change from one pattern to another (AB to AA, where AA denotes

80 the 2D ice structure) depending on the pressure applied in the system[22, 27]. A similar structure
81 pattern change was also revealed for water in a non-uniform confinement, such as in the gap
82 between the tip and the substrate of an Atomic Force Microscope (AFM) device. In the latter case,
83 localised 2D ice structures, the so-called "nano-ribons", were observed[26]. These structures depend
84 on how well water atoms fit in the nano-size gap of a solid material, i.e. whether the characteristic
85 size of individual water atoms is commensurate with respect to the gap or not. This leads to
86 different solid-like structures, e.g. monolayer, bilayer, tri-layer, or a diffuse layer typical of liquid
87 water. In turn, these localised water structures lead to rapidly changing material properties thereby
88 enabling a discontinuous local friction force that produces the “stick-slip” motion of lubricated
89 surfaces, as reported in the experiments[29]. Furthermore, recent MD simulations of a stack of
90 parallel graphene sheets immersed in water[30] reported the deformation of planar graphene layers
91 into surface ripples. The ripples are a result of the graphene sheet flexibility and the effect of Van
92 der Waals forces between graphene and water, which leads to a non-uniform water confinement.
93 In comparison with the fixed non-uniform confinement in the AFM experiment case, the
94 graphene/water interaction process is dynamic: the rheology of the graphene layer changes due to
95 response from the water atoms, which leads to bending of the graphene sheet, which, in turn,
96 triggers new phase transitions in water, and so on[31]. In this case, mobile areas of graphene ripples,
97 the so-called “dripplons” are formed, which show unusual transport properties, such as a very large
98 diffusion velocity.

99 Despite recent progress in the understanding of the role of nano-confined water phase transitions
100 on water/hydrophobic surface interaction, many existing investigations in the literature have been
101 limited to systems at equilibrium conditions, that is, no flow case. For example, because of the
102 absence of flow, the slip length in nanoconfined water systems cannot be computed from

Equilibrium Molecular Dynamics (EMD) simulations directly. Instead, the slip length is computed as a ratio of the viscosity coefficient and the friction coefficient[32-33]. In comparison with the slip length, viscosity can be calculated from EMD simulations using the Green-Kubo method[21, 34]. Results of the shear viscosity coefficient calculation from several EMD simulations are summarised in Table 3. It can be noted that predicted the shear viscosity coefficients tend to increase with the water confinement. The suggested viscosity increase for sub-nanometer confinement is especially drastic. However, it should be reminded that the Green-Kubo (G-K) relation was derived for bulk liquid systems and its validity in application to water under strong confinement is not guaranteed[35-40]. Furthermore, for an EMD simulation of the nano-size water slab confined between graphene layers, the G-K method results may not be reliable. As discussed in Supplementary Information III, in this case the tails of the autocorrelation function at large time separations show a very slow non-monotonic decay and the corresponding integral under the curve does not converge.

Table 3. EMD predictions for change in water shear viscosity coefficient under confinement by a hydrophobic material

Reported by	Change in water system size, nm (diameter of CNT or slit width of graphene channel)	Obtained results for the shear viscosity coefficient, Pa·s
Ye et al.[41]	0.8 to 5.4	Decreases from 5.6×10^{-4} to 2.6×10^{-4}
Babu et al.[42]	1.2 to 5.4	Decreases from 4.5×10^{-4} to 0.5×10^{-4}
Shaat et al.[43]	1.3 to 9.7	Decreases from 6.8×10^{-4} to 3.2×10^{-4}
Chen et al.[44]	0.675 to 4.053	Decreases from 10^{-6} to 10^{-8}
Neek-Amal et al.[21]	0.75 to 2	Non-monotonically decreases from 10^{-1} to 8.8×10^{-4}

Both slip length and viscosity of molecular liquids at nano-confinement conditions can also be obtained from Non-Equilibrium Molecular Dynamics[33, 45-46] (NEMD). In comparison with EMD, NEMD explicitly includes flow in the simulation. However, up until present, NEMD simulations of nano-confined water have been limited to calculations of the slip length only (Table 4) while both the viscosity and the underlying water molecular structure, which formed in the process, received little attention.

Table 4. NEMD predictions for change in water slip length under confinement by a hydrophobic material

Reported by	Range of strain rates, s^{-1}	Change in water system size, nm	Trend in slip length, nm
Ramos-Alvarado et al.[33]	1×10^{11} to 12×10^{11}	3 to 8	Decreases from 30 to 20 for all strain rates
Wagemann et al.[45]	10^{8} to 10^{9}	2 to 2.8	Increases from 50 to 125 for all strain rates
Kannam et al.[46]	1.79×10^{10} to 25.6×10^{10}	3.9	Values in the range from 65 to 115

Table 4 shows no consensus for predictions of the NEMD simulations for the slip length in nano-confined water systems even in terms of the trend. This lack of agreement can be explained by the fact that in comparison with the experiment, NEMD usually has to operate at unrealistically high flow rates to overcome the statistical noise problem. The noise occurs as the result of insufficient ensemble averaging in case of a microscopically small space and time domain of the molecular dynamics simulation when calculating the meanflow velocity gradients from MD results. Unless the meanflow velocity gradient is in order of THz it is difficult to accurately separate it from noise due to the insufficient averaging of thermal velocity fluctuations. On the other hand, very high

shear rates require an extra care when performing NEMD simulations and interpreting their rults[8, 33, 46].

This gives motivation to the present work which aims to investigate how the flow and structure properties of water depend on the gap between graphene walls. A systematic NEMD campaign is performed to include a non-uniform flow in the simulation while keeping the simulation errors under control. The shear flow of water in a nano-size slit between two graphene walls is initiated by moving one wall tangentially to another in accordance with the steady Couette flow conditions. Several molecular dynamics models of water and graphene walls (different MD potentials, different MD ensembles, different layer structure of graphene walls) are considered in accordance with recommendations in the literature. The simulation results from the different models are compared to probe the results' sensitivity to numerical parameters. Furthermore, the effect of the size of the molecular dynamics simulation domain on the observed structural and hydrodynamic properties of the nano-confined system is analysed. Finally, simulations in a wide range of velocity strain rates accessible to NEMD are conducted and the results are extrapolated to the kHz region, which would be of interest to experimentalists.

RESULTS

1. Steady Couette problem

A slab of water is placed between two parallel graphene sheets aligned with the x-y plane (Fig.1). A Couette flow is started by impulsively moving the top graphene sheet relative to the bottom well at a constant velocity in the x-direction thereby generating a shear velocity gradient in the wall-normal direction, z. The stationary solution is obtained by running molecular dynamics simulations over a sufficiently long time, 1 ns, to eliminate transients from the solution and then run for another 10-90 ns for statistical averaging. Both the width of the water slab and the velocity of the moving

159 graphene sheet are varied in order to investigate the effect of different strain rates under a range of
160 confinements from sub-nanometer to several nanometers where water is expected to demonstrate
161 standard bulk liquid properties.

162 The number of graphene layers in the graphene sheets is also a parameter of the model because
163 previous research for other nano-confined molecular liquids such as liquid argon showed the
164 importance of the Van der Waals forces for nanometer-size argon slabs, which affects transport
165 properties such as slip length[47]. Furthermore, previous studies also used multi-layer graphene sheet
166 models for the NEMD simulation of nano-confined water[46, 48]. Despite these previous
167 investigations, it should be noted that the present work is the first time when the effect of the
168 number of layers in the graphene sheet on the transport properties of nono-confined water has been
169 systematically studied in NEMD simulations. The multi-layer model is implemented by treating
170 the two outermost graphene layers as rigid surfaces whose coordinates are calculated in accordance
171 with the analytical Couette solution. Two areas of the computational domain in the (x-y) plane are
172 considered: 3.5 x 3.6 nm^2 and 8 x 8 nm^2 to investigate the NEMD model sensitivity to the domain
173 size. All internal graphene layers remain flexible and are simulated in accordance with the
174 molecular dynamics potentials for graphene-graphene and graphene-water interactions.

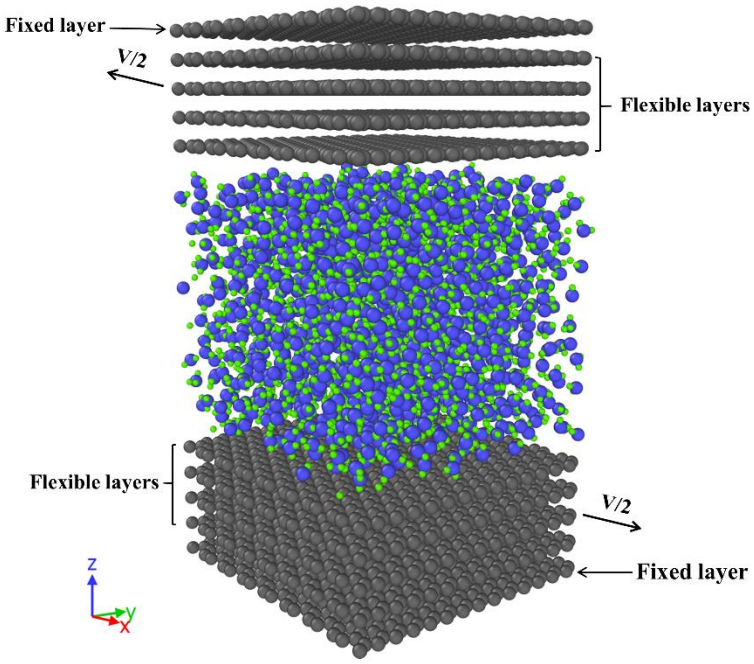

Fig.1 NEMD simulation domain for the graphene-water Couette problem.

2. Configuration of the NEMD model

A suitable choice of molecular dynamics potentials for the nano-confined Couette problem has been identified to include the flexible-bond model SPC/Fw for water, optimized Tersoff for carbon atoms of graphene sheets, and a suitably modified Leonard-Jones (L-J) potential for graphene-water interactions (see details in the Methods).

For a specified temperature and number of atoms in the system, two typical choices are to conduct molecular dynamics simulations for a conserved volume (NVT ensemble) or a conserved pressure (NPT). The NVT approach allows one to precisely control the distance between the graphene sheets thereby preserving the density of the nano-confined water in this slit. For sub-nanometer confinement, such precise control of local water density is very important for capturing the liquid-to-solid state water transition that critically depends on how commensurate water atoms

188 are with the slit size as discussed in the introduction. However, in this case the normal pressure
189 force exerted on the graphene sheets is not controlled and reaches very large values order of GPa.

190 The alternative NPT approach does allow one to preserve a constant pressure (e.g. equal to
191 atmospheric) by applying a local barostat model to the graphene wall atoms[49-50]. The barostat
192 works by artificially adjusting the distance between the two graphene sheets at each time step
193 thereby modifying the local density of water atoms accordingly. The modification is very
194 significant for sub-nanometer slit sizes and the NPT model fails to reproduce the liquid-to-solid
195 water transition in comparison with the experimental observations for such systems (Supporting
196 Information I, Parts 1-4). Hence, despite the large values of pressure obtained in the system, the
197 NVT model is selected as the molecular dynamics approach of choice for simulations here.

198 The next step is to establish a trade-off between the accuracy of NEMD simulations and the
199 computational cost of the model by adjusting the number of layers in the graphene sheet to an
200 appropriate number. This is achieved by performing simulations at different numbers of graphene
201 layers per sheet, from 2 to 6 and comparing the results for slip length and shear viscosity for
202 different slit widths and strain rates. Both quantities are computed from the meanflow velocity
203 distribution of water in the wall-normal direction, using the Newtonian flow assumption and using
204 the averaging in time and over the statistically homogeneous directions, x and y (further details
205 are in Methods and Supporting Information II, Part 1 and 2)

206 Fig.2a and b shows the distributions of slip length obtained for water flows inside the 3.8 nm
207 and the 0.8 nm size slit, respectively. The strain rate is varied in each case and its values are
208 significantly higher than currently realizable in the experiment. The high rates are essential for
209 keeping the MD simulation cost feasible, as discussed in the introduction.

In the 3.8 nm slit case, which corresponds to a relatively large thickness of the water layer where the nano-size confinement effects are not too important, the results show that the slip length virtually remains constant with respect to the strain rate. This is consistent with the previous MD study[33] that reported a constant slip length of water under a range of velocity strain rates from 12×10^{10} to 40×10^{10} s^{-1}. The same trend is also confirmed in the experiment[51] for a similar size slit between the graphene layers (but at much lower strain rates).

For the 0.8 nm slit width, the slip length increases with the strain rate. Importantly, the slip length increase in this case is sufficiently above the error bar of the MD simulations (see Supporting Information I, Part 6), hence, the reported variation is significant.

It can be noted that the increase of the slip length with confinement is consistent with some of the previous studies (Table 4). Furthermore, the previously mentioned lack of consensus in the NEMD literature on the slip length behaviour as a function of the velocity strain rate[47, 51-54] for the nano-size confinement, at least partially, can be attributed to the effect of the number graphene layers on the graphene/water interaction. For example, previous NEMD simulations of graphene/water systems with large slits[33, 45-46] predicted the slip length in a range from 20 to 125 nm. This is consistent with the results of the suggested NEMD model with two layers per graphene sheet at the 3.8 nm slit width, which predicts the slip length of about 20 nm. However, the predicted value is too large in comparison with in the graphene/water experiments[12-14] which reported the slip length between 8 and 12 nm[12-14]. In the suggested NEMD model, once the number of graphene layers is increased to 4-5, the results for the lip length fully agree with the experiment.

In comparison with the 3.8 nm slit MD models, the slip length results of the 0.8 nm slit system are much less sensitive to the number of layers in the graphene sheet. This difference is an

indication of the structural change of graphene/ water interactions which occur in the case of sub-nanometer size confinement.

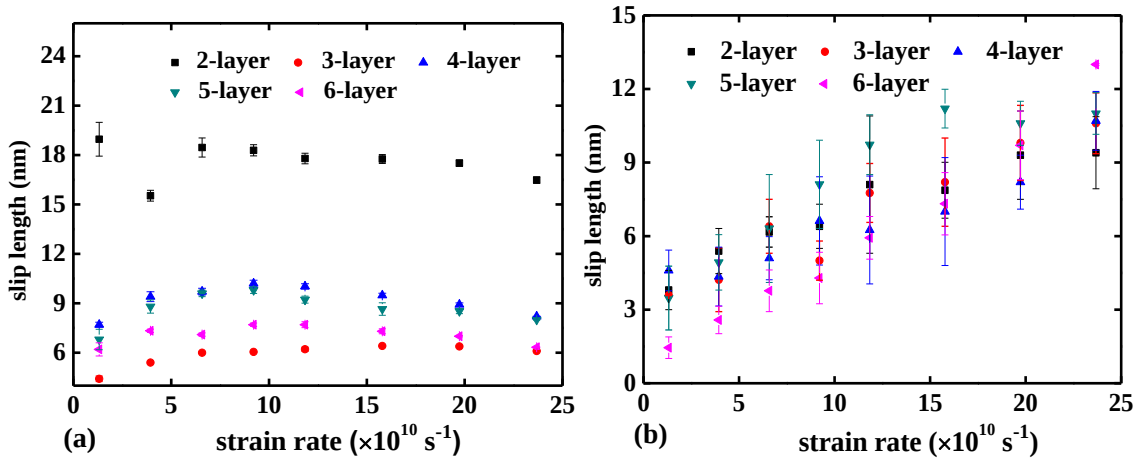

Fig.2 Dependence of the slip length of water on velocity strain rate for different numbers of layers per graphene sheet at (a) 3.8 nm and (b) 0.8 nm slit width.

Fig.3 shows the resulting distributions of the dynamic shear viscosity coefficient μ of water as a function of the strain rate for the same slit widths, 0.8 nm and 3.8 nm and for different numbers of graphene layers (comp. with Fig.2). In each case, the computed shear viscosity coefficient is normalised by the bulk water viscosity value at room temperature[55]. As expected, for moderate velocity strain rates in the large slit of 3.8 nm, the shear viscosity coefficient is close to the bulk value (Fig.3a). For high strain rates, in accordance with the literature[56-57], water exhibits a shear thinning behaviour so that the shear viscosity coefficient μ decays with the shear rate. Fig.3b shows that, for the 0.8 nm slit case, the viscosity coefficient becomes 2 to 3 times larger than the bulk value. In contrast to the large slit case, there is no clear dependence on velocity strain rate observed for the small slit case. The notable amplification of water viscosity under the sub-nanometer slit is another manifestation of the liquid-to-solid water transition that occurs when the

slit width reduces from 3.8 nm to 0.8 nm in consistence with previous EMD investigations[58] and the experiment[57, 59].

Interestingly, in comparison with the slip length, there is no strong dependency of the shear viscosity coefficient, μ on the number of layers in the graphene wall model even in the 3.8 nm slit case. This can be explained by the fact that molecular viscosity is an average volume property whereas the slip length mainly depends on the water/graphene interface forces. These forces depend on the interplay of Van der Walls forces and the flexibility of graphene layers in the normal direction.

In summary, to correctly calculate both the slip length and the viscosity coefficient for the large slit case in comparison with the reliable experimental data available, the five-layer graphene-water model is selected for all further NEMD simulations in this article.

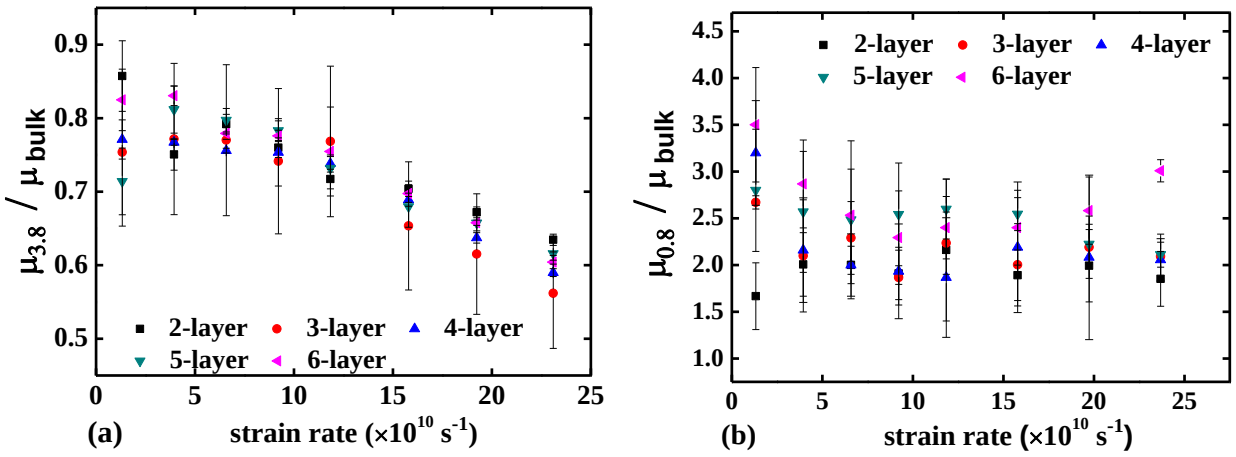

Fig.3 Dependence of the shear viscosity coefficient of water on velocity strain rate for different numbers of graphene per graphene sheet at (a) 3.8 nm (b) 0.8 nm slit.

3. The confinement effect on normal stress differences

In the non-Newtonian flow literature[60], normal stresses are used to characterise the deviation of the shear stress-strain behaviour from a linear relationship. In continuum mechanics, the maximum

shear stress is equal to one half of the applied normal stress when the angle between the normal force and the shear direction is 45°. For Newtonian systems with a rotational symmetry, like the current nano-confined water system where the shear is applied in the normal direction to the graphene wall (z-direction), this means $\frac{1}{2} \times \left(\tau_{xx} - \tau_{yy}\right) = \tau_{x'y'} = 0$, where (x', y') corresponds to the rotated coordinates of the stress tensor in (x, y) plane.

In order to investigate how the effect of sub-nanometer confinement affects the Newtonian property of water between the graphene sheets, Fig.4 compares the distribution of the first normal stress difference $\frac{1}{2} \times \left(\tau_{xx} - \tau_{yy}\right)$ as a function of velocity strain rate for the 3.8 nm and the 0.8 nm slit systems. Here τ_{xx} and τ_{yy} are the normal stresses in water which can be calculated from the virial stress relationship[61] (Supporting information II, Part 3).

In agreement with the continuum theory, the simulation of the 3.8 nm slit case reveals that the water interaction with the graphene sheet has a negligible effect on the rotational symmetry of the water system: the first normal stress difference is virtually zero for all velocity strain rates. In comparison with this large slit case, for 0.8 nm slit, the first normal stress difference is notably amplified. Again, this suggests that the water in the 0.8 nm slit underwent a state change in comparison with the 3.8 nm slit case.

Despite the difference in the graphene sheet/water response, it can be also noted that in both these cases the normal stress difference is virtually independent on the out-of-plane strain rate as expected for a Newtonian fluid. This justifies the use of the standard method for calculating the shear viscosity coefficient as discussed in Methods.

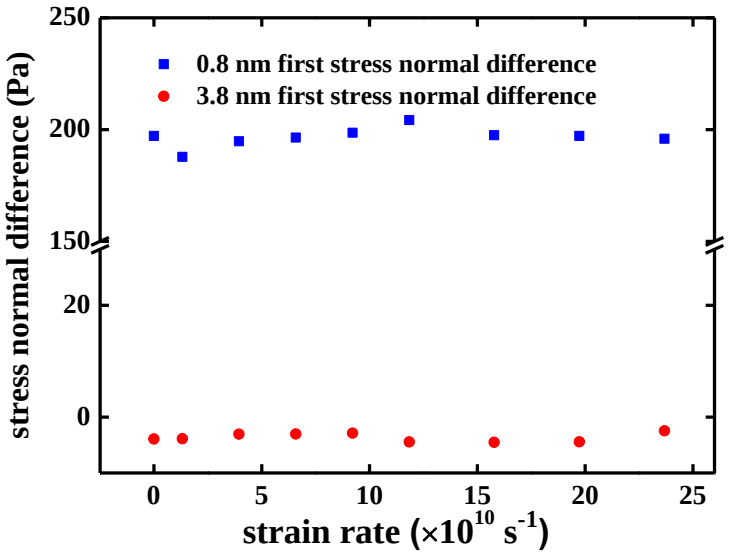

Fig.4 Dependence of first normal stress difference on the velocity strain rate for different slit widths between the graphene sheets.

4. The effect of graphene confinement on water state

In order to understand the origin of the differences, which occur in mechanical properties of the nano-confined water when the slit width reduces from 3.8 nm to 0.8 nm, instantaneous snapshots of molecular structures in both cases are compared. Fig.5a shows the atomistic structure of water in the centre of the 3.8 nm slit. The water structure is amorphous as typical of liquids. In contrast to this, for the 0.8 nm slit case, Fig.5b shows the presence of layers of 2D ice, which is similar to the square ice structure reported in the EMD literature[22] that forms in a sub-nanometer confinement. Furthermore, Fig.5b shows the formation of a monolayer ice structure in Zone I and Zone III while bilayer ice exists in Zone II, where the slit gap between the top and the bottom inner graphene layers opens up slightly wider. The variation of water solid-states is similar to the previous reports of the nano-ribon ice structure under non-uniform confinement[26, 31]. In the current case, the non-uniform confinement is caused by deformation of the graphene layers and attributable to the Van der Waals forces at the graphene/water interface. As was previously

reported in the EMD literature for zero flow case[31], it is the interplay of the Van der Waals forces and the subsequent graphene bending deformation response that leads to a coexistence of monolayer and bilayer ice structures between flexible graphene layers.

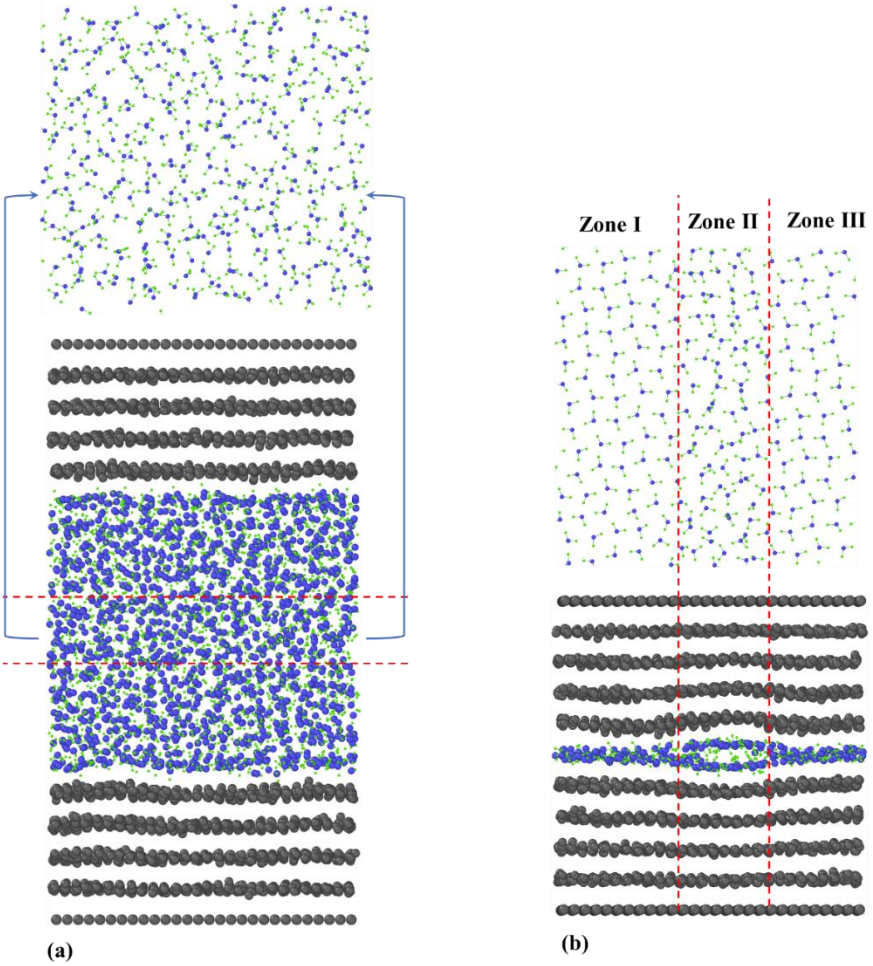

Fig.5 Atomistic structure of water confined between the graphene layers for the 3.8 nm (a) and the 0.8 nm (b) slit cases at a strain rate of 23.68×10^{10} s^{-1}. The snapshots on the top are the top view and those on the bottom are for side view. The top view corresponds to a slab of water of the size of the small gap (0.8 nm) extracted from between the graphene layers as shown. Monolayer ice is formed in Zone I and Zone III, while bilayer ice is formed in Zone II, which corresponds to the graphene layer "ripples".

311 Following[31], the graphene layer bending / Van der Walls force interaction could be expected to
312 be a dynamic process. Hence, in order to answer the question if the time scale of the evolution of
313 “ripples” in graphene layers is important in comparison with the atomistic time scales and also to
314 prove that the graphene layer deformation was not an artefact of large velocity strains applied in
315 the NEMD model, a separate equilibrium molecular dynamics (EMD) simulation is performed for
316 the same system. In this EMD simulation, water is confined by stationary graphene walls which
317 are separated by a 0.8 nm slit. The simulation is run for a sufficiently large time (30ns) to
318 investigate the long-time behaviour of the “ripples”. Fig.6 shows snapshots of the resulting
319 atomistic graphene/water structure at different time moments in the *y-z* plane. It can be seen that
320 the bilayer region is separated by two monolayer zones and slowly diffused between the graphene
321 walls. Notably, the increase of the molecular dynamics simulation domain by a factor of 2 in each
322 x and y direction, from 3.5 x 3.6 nm^2 to 8 x 8 nm^2 area of the graphene sheet, while keeping the
323 same slit width equal to 0.8 nm, does not change either the structure of the “ripples” or their
324 diffusion time. Animations of the graphene-water system are provided in Supporting Information
325 IV and V.

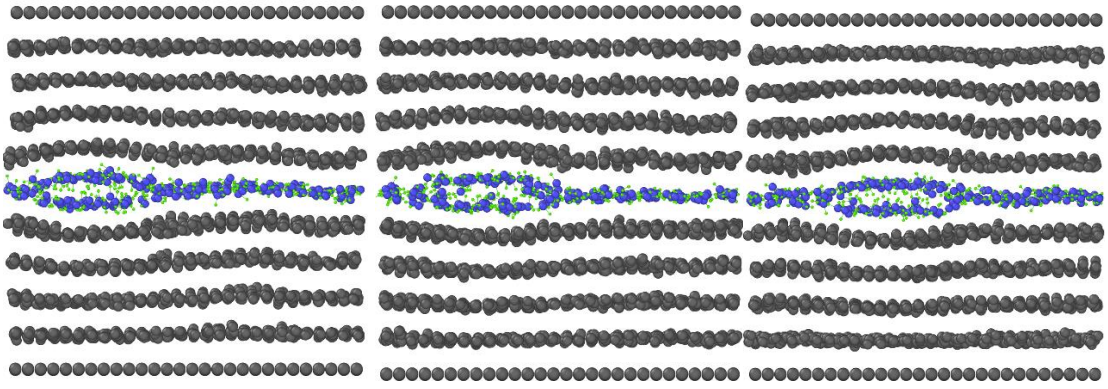

326

327 t=1 ns t=10 ns t=30 ns

Fig.6 Slow diffusion of the graphene layer "ripples": snapshots of the atomistic structure of nano-confined water inside graphene layers with 0.8 nm slit as obtained from equilibrium MD simulations for zero flow.

Having established that diffusion of the graphene layer "ripples" is a slow process in comparison with molecular dynamics times, another question to answer is if material properties of the nano-confined graphene/water system depend on local rheology details such as the orientation of the "ripples" of the deformed graphene layer. In order to answer this question additional NEMD simulations were performed for the graphene layer "ripples" aligned with the flow direction and at 90^{o} angle to it. The obtained results confirm that both the transport and the atomistic structure properties of nano-confined water are more-or-less insensitive to the orientation of the "ripples" on the graphene layer with respect to the flow (Supporting Information VI).

5. The effect of confinement on water dynamics

The next step is to investigate transport properties of the nano-confined graphene-water system for a variable slit width while keeping the velocity strain rate constant and equal to a high value 23.68×10^{10} s^{-1}. The latter is to reduce the MD simulation run time required for a sufficient statistically averaged solution without notable thermal noise effects.

Fig.7a shows that the slip length tends to increase as the slit decreases, in agreement with some of the previous literature (comp. with Table 4). The decrease is non-monotonic with emerging oscillations especially notable for slit widths smaller than 1.5nm, which can be attributed to non-continuum water effects. A qualitatively similar trend is also observed for the shear viscosity coefficient, μ. The latter is about 0.7-1 of the bulk water viscosity at moderate to large slits of

1-3.8 nm and then becomes amplified by a factor of 2 of the bulk value once the slit width reduces to 0.8 nm (Fig.7b).

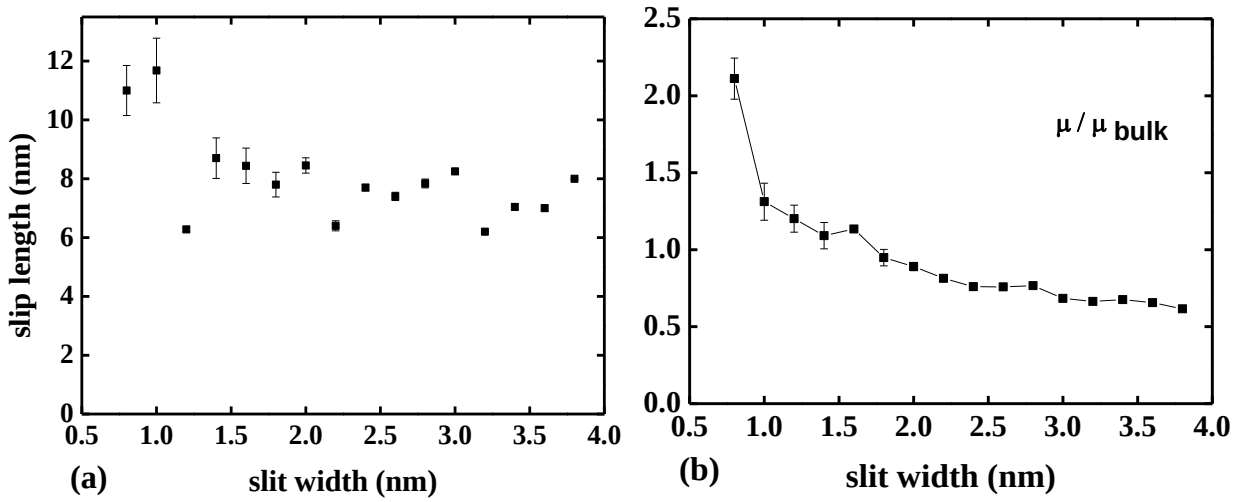

Fig.7 Distribution of (a) slip length and (b) shear viscosity as a function of the slit width at a fixed strain rate of 23.68×1010 s-1.

The predicted increase of the shear viscosity for sub-nanometer confinements is several orders of magnitude smaller in comparison with predictions of some recent equilibrium molecular dynamics simulations based on the Green-Kubo (G-K) method for viscosity calculation[21] as well as the results of the AFM experiment[12]. It should be recalled that both the G-K and AFM results for shear viscosity can be debated as discussed in the introduction. Nevertheless, since the extremely high strain rates applied in the NEMD calculations remain a potential culprit for discrepancies with the EMD results, an additional series of simulations was performed with the standard, 3.5 x 3.6 nm^2 and the increased, 8 x 8 nm^2 area of the graphene sheets for several slit widths and for a range of velocity strain rates.

The results for the standard-size and the increased-size computational domains are similar and in what follows the result for the 8 x 8 nm^2 graphene sheets are shown.

Fig.8 demonstrates the slip length distribution as a function of the strain rate for the 0.8 nm slit width (Fig8a) and for the 3.8 nm slit width (Fig.8b). Fig.9a and b shows the distribution of the shear viscosity coefficient as a function of the strain rate for the same two slit widths. And Fig.10a and b shows the corresponding distributions of the friction coefficient that is a ratio of the shear viscosity to the slip length.

First of all, in can be noted that, for all three quantities, there is a qualitative change between the response to shear of the graphene/water system with 0.8 nm slit from that with 3.8 nm slit. Interestingly, this change occurs when the slit width reaches sub-nanometer. On the other hand, the variation of the slip length, viscosity and friction coefficient for slit width between 3.8 nm and 1.0 nm are similar (for details of water transport properties in 1.0 nm slit see Supporting Information II, Part 4).

In case of the sub-nanometer slit width for relatively low strain rates, the slip length shows a decrease with the slit width decrease. In comparison with this, both the viscosity coefficient and the friction coefficient show a rise as the shear reduces despite the non-monotonic behaviour of the viscosity coefficient at high strain rates. Hence, it can be speculated that for standard laboratory conditions corresponding to the experiments of Table 2 which operate at velocity strain rates order of kHz, which is much lower in comparison with NEMD, the viscosity coefficient may further increase. In order to investigate this further, approximate valuates of the shear viscosity coefficient for both the 0.8 nm and the 3.8 nm slit widths at 1 kHZ strain rate have been obtained by extrapolation of the NEMD results at three lowest available strain rates, 1.32×10^{7}, 3.94×10^{7} and 6.58×10^{7} kHz. The extrapolation results together with the uncertainty band are summarised in Table 5. It can be noted that the shear viscosity values extrapolated to 1 kHz do not depend on the size of the model within the uncertainty bar. The results of the NEMD modelling for the large slit

width underpredict the bulk viscosity value by about 30%. On the other hand, the obtained results for the 0.8 nm slit width show 4- to 5-fold shear viscosity increase in comparison with the bulk value. However, this increase is still too small in comparison with the shear viscosity increase reported in the experiments (Table 2).

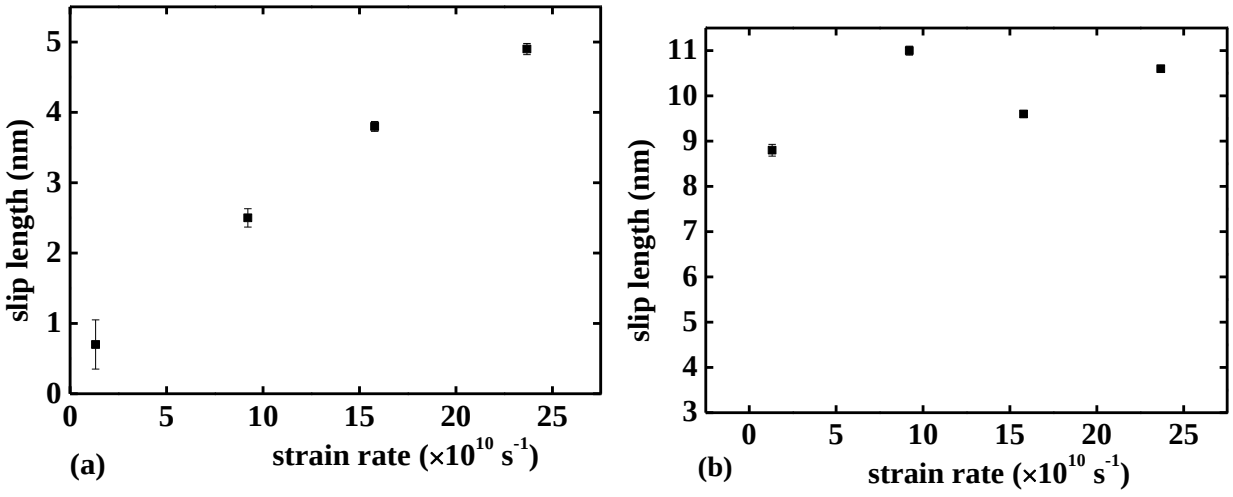

Fig.8 Variation of the slip length as a function of the velocity strain rate in the graphene channel for (a) 0.8 nm and (b) 3.8 nm slit widths.

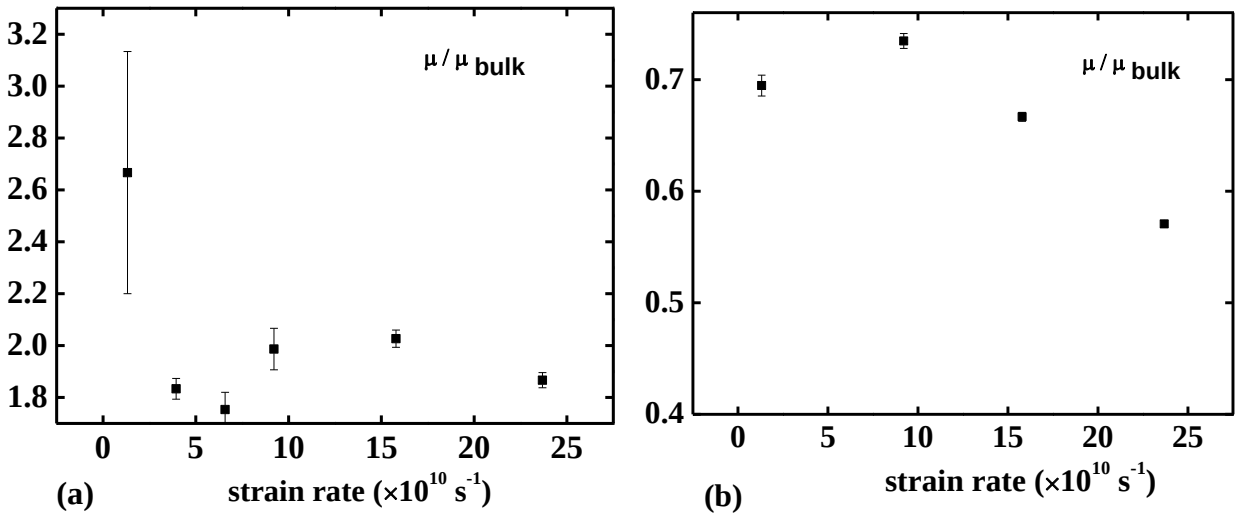

Fig.9 Variation of the shear viscosity coefficient as a function of the velocity strain rate in the graphene channel for (a) 0.8 nm and (b) 3.8 nm slit widths.

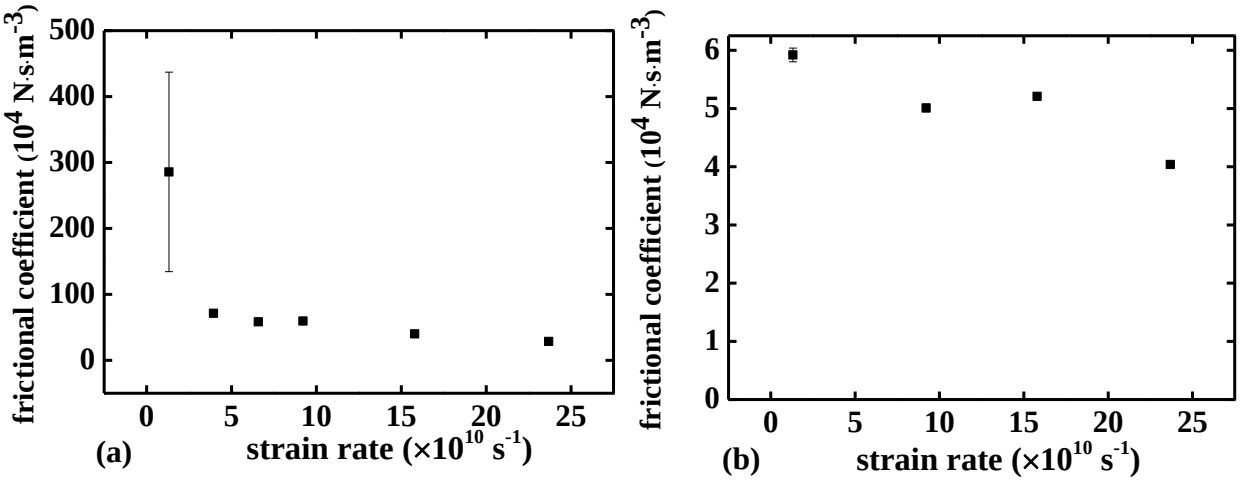

Fig.10 Variation of the frictional coefficient as a function of the velocity strain rate in the graphene channel for (a) 0.8 nm and (b) 3.8 nm slit widths.

Table 5. NEMD results for shear viscosity extrapolated to 1kHz strain rate

Model size	8 x 8 x 0.8 nm^2	3.5 x 3.6 x 0.8 nm^2	8 x 8 x 3.8 nm^2	3.5 x 3.6 x 3.8 nm^2
μ/μ_{bulk}	3.37±0.85	2.97±0.73	0.68 ±0.01	0.623±0.05

It is further instructive to compare the above NEMD results with the shear viscosity coefficient which has been obtained for the same system using the standard EMD simulation for the no-flow case (Supplementary Information III). The obtained viscosity coefficients for different slit widths are summarised in Table 6 with and without using the conventional rotational symmetry assumption to simplify the Green-Kubo integral by expressing various shear stress terms via the normal stress differences[37]. The EMD results show a strong dependency on the integration time of the auto-correlation function of the Green-Kubo method, which has very "heavy" tails especially

410 in the case the conventional rotational symmetry assumption. Apparently, the corresponding
411 numerical integrals do not converge over the range of time separations amenable to molecular
412 dynamics solution averaging.

413 **Table 6. EMD results for shear viscosity as a function of the integration time**

	0.8 nm		3.8 nm	
	Integration time 10 ps	Integration time 20 ps	Integration time 0.2 ps	Integration time 0.4 ps
GK no diagonal term	0.6	0.7	0.064	0.1
GK with diagonal term	3.7	6	0.11	0.21

414

415 Now turning our attention to address the lack of agreement with the experimental data in Table 2,
416 which shows a large increase of the viscous force at sub-nanometer confinements, let us compare
417 the effect of the strain rate on the shear force exerted on the graphene sheet for different slit widths
418 (Fig.11a) with the that on the normal force (Fig.11b). It can be seen that the shear force only weakly
419 depends on the slit width unless the strain rates is very high. On the other hand, the magnitude of
420 the shear force depends on the strain rate approximately linearly is in accordance with the expected
421 behavior of a Newtonian fluid (see discussion in Section 3). In comparison with this, the normal
422 force acting on the graphene sheet exhibits a sharp rise in the vicinity of one-nanometer slit width,
423 which corresponds to at least a factor of 20 amplification in comparison with the "bulk" value
424 associated with moderate to large slit widths (> 3 nm). This rise is non-monotonic and likely to be
425 driven by non-continuum effects such as how commensurate or non-commensurate the distance
426 between two layers of water atoms is in comparison with the slit width (see introduction).
427 Importantly, the rise of the normal force is completely independent of the strain rate, which

suggests that the water transition from liquid to solid-like state is independent of the velocity strain rate either. Indeed, a series of additional EMD simulations performed for zero flow led to virtually the same result as NEMD (Fig.11b). Hence, it can be expected that unless the *local* tangential and normal forces, which are exerted on the graphene sheet of a nano-confined system, are well resolved in an experiment, so that the product of the normal force and the small angle corresponding to the deviation from the assumed parallel set-up is much smaller than the shear force magnitude (see Supplementary Information III), the value of shear viscosity coefficient estimated from the experiment should be treated with caution. Furthermore, it can be speculated that the effect of graphene layer rheology due to the emergence of "ripples" at the graphene/water interface is to increase the effective slip length thereby competing with the effect of shear viscosity increase under the sub-nanometer confinement.

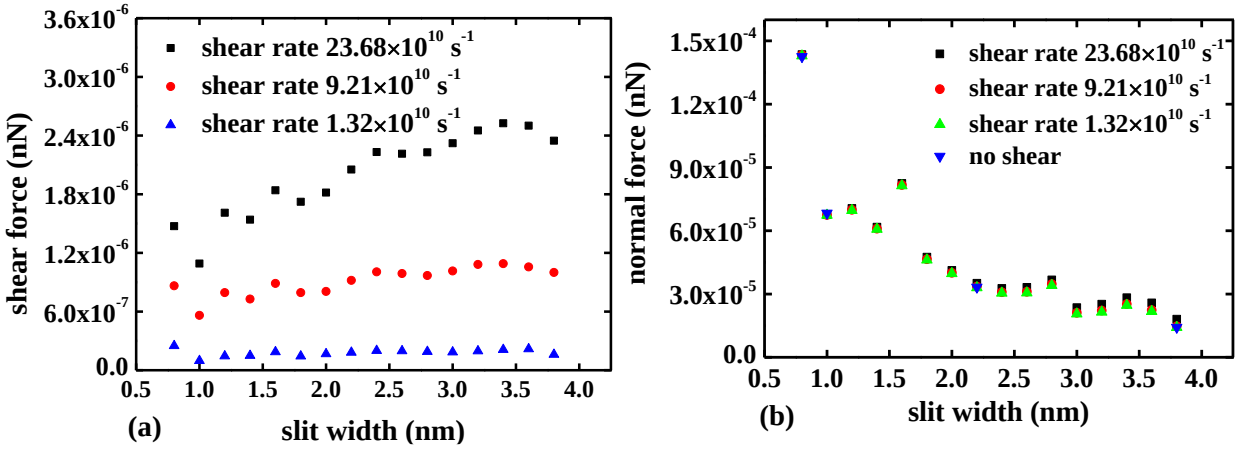

Fig.11 Variation of the shear force (a) and normal force (b) on the graphene sheet as a function of the slit width and the velocity strain rate in the graphene channel.

6. The effect of shear flow on radial distribution functions in liquid-like and solid-like water

In order to further analyse changes in the nano-confined water properties when the slit width between the graphene layers reduces to sub-nanometer, the atomistic structure of nano-confined

445 water is analysed next. Fig.12 shows lateral radial distribution functions (LRDF) of water atoms
446 in the plane parallel to the graphene walls for different slit widths (see Methods for the definition
447 of LRDF). In each case, the velocity strain rate is fixed to a constant equal to 23.68×10^{10} s^{-1} for
448 the sake of computational efficiency.

449 Fig.12a demonstrates the LRDF results for oxygen-oxygen. The same distributions for oxygen-
450 hydrogen are shown in fig.12b. In comparison with larger slits, a drastic change in both LRDF
451 distributions occurs when the gap between the graphene layers reduces from 1.0 nm and 0.8 nm.
452 For example, in the case of the 0.8 nm slit, multiple peaks emerge in the water structure which is
453 typical of the hydrogen bond network. In comparison with the large slit case, the second peak of
454 the LRDF distribution of the 0.8 nm slit model moves to smaller radial distances r_{xy}, which
455 indicates a stronger hydrogen bond formed in second shell. Interestingly, while the position for the
456 first peak remains unchanged, its peak is amplified. This suggests that more atoms are located
457 within the radial distance of the first peak in the 0.8 nm case in comparison with the larger slits
458 where the water structure is liquid-like. Notably, the stronger hydrogen bond in the second shell
459 and the unchanged position for the first peak are in agreement with previous EMD simulations of
460 nano-confined water[58] which reported a similar solid-like water behaviour under strong
461 confinement. The similarity between the NEMD and the previous EMD results suggests
462 independence of the solid-like water structure of the applied velocity strain rate in the solid-like
463 water, which is also consistent with the discussion in Section 5 (comp. with Fig.11b).

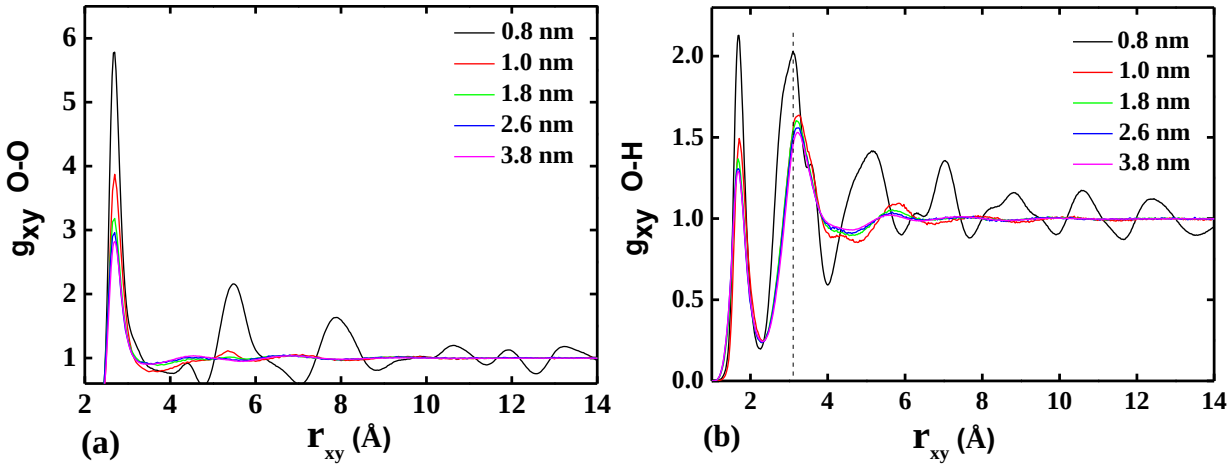

Fig.12 Dependence of lateral radial distribution functions (LRDF) of nano-confined water on the slit width for (a) oxygen-oxygen and (b) oxygen-hydrogen interactions. LRDF is computed in a plane parallel to the graphene layers and a constant velocity strain rate of 23.68×10^{10} s^{-1} is applied. The vertical dash line in (b) demarcates the location of the second peak of LRDF for the 0.8 nm slit case.

In order to analyse how the shear flow affects the nano-confined water structure, Figs. 13 and 14 show how the LRDF distributions of water atoms in the x-y plane evolve as a function of the strain rate for the 3.8 nm and the 0.8 nm slit case, respectively. The presented results correspond to the model with the graphene sheet area of 3.5 x 3.6 nm^2. The LRDF results obtained for the same two slit widths and the large computational domain corresponding to the graphene sheet area of 8 x 8 nm^2 are similar.

In the 3.8 nm slit, water behaves as liquid. In this case, LRDF structure of both the oxygen-oxygen and the oxygen-hydrogen becomes more diffuse as the velocity strain rate increases. Here the peaks and the valleys of the radial distribution gradually reduce as the strain rate grows larger. Such behaviour can be associated with the shear thinning effect of water at large strain rates (comp. with Fig.9b). On the other hand, the locations of peaks and dips of the radial distributions are

invariant of the strain rate. The latter suggests that intermolecular forces, such as those acting between the water atoms and the graphene walls, are not affected by the shear flow gradient. The last point is also consistent with the previous observation that the slip length on the graphene wall is more-or-less independent of the velocity strain rate in the large slit case (comp. with Fig.8b). Additional MD simulations of the large slit case confirm that the revealed effects do not depend on the choice of MD force field, e.g. either with a flexible or a rigid bond water model, which are both equally applicable for liquid-state water simulations (Supporting Information I, Part 5).

In comparison with the 3.8 nm slit case, the water assumes a solid-like state in 0.8 nm slit. In the latter case, the long-range order of radial distributions of all inter-atomic interactions is completely independent on the velocity strain rate. The ice structure developed in the slit in this case is sufficiently rigid to resist any deformation under the applied shear force. This solid-like behaviour is consistent with a gradual increase of the slip-length with the velocity strain rate observed earlier (comp. with Fig.8a). The slip length change with the strain rate is indicative of a weaker interaction between the water atoms and the graphene wall in comparison with the interatomic forces of the condensed-state water that behaves like a solid crystal sliding between the two graphene sheets.

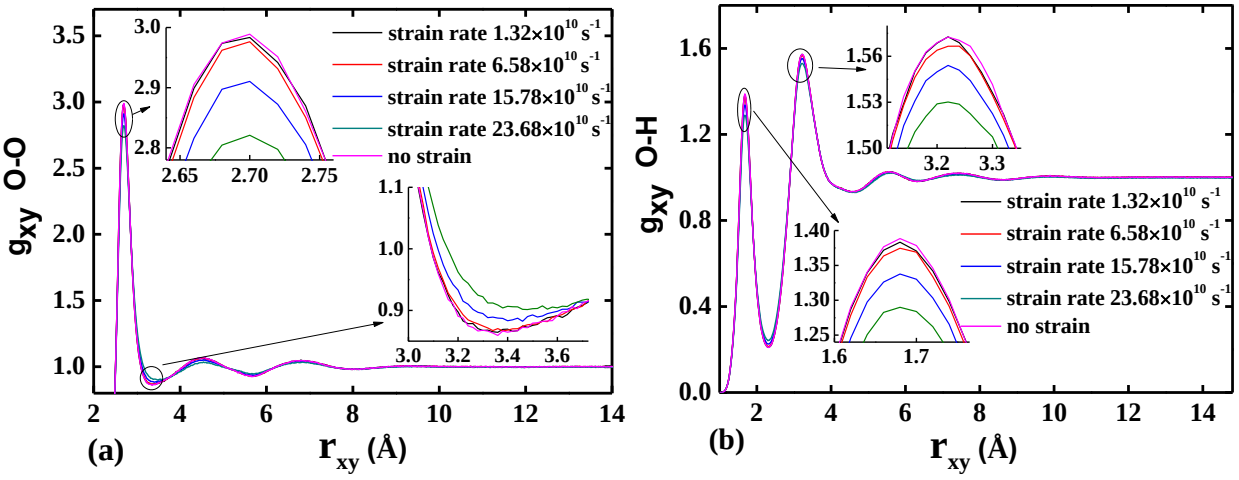

Fig.13 Lateral radial distribution functions (LRDF) of (a) oxygen-oxygen and (b) oxygen-hydrogen interactions of water in a plane parallel to the graphene walls for the 3.8 nm slit width at different strain rates. The insets in (a) are zoomed-in views of the first peak and the first valley of the radial distribution function. The insets in (b) show a zoomed-in view of the first and the second peak.

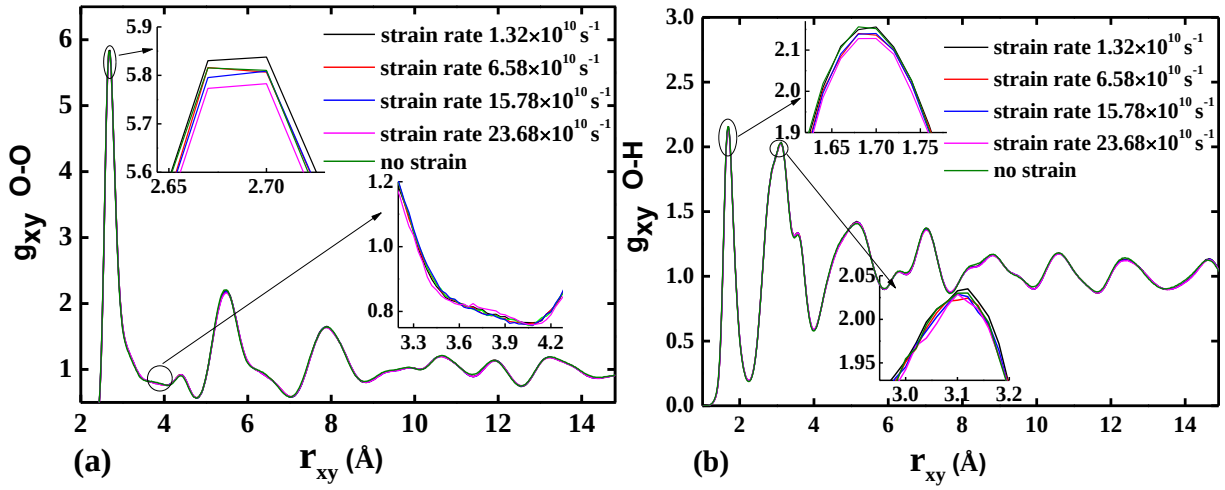

Fig.14 Lateral radial distribution functions (LRDF) of (a) oxygen-oxygen and (b) oxygen-hydrogen interactions of water in a plane parallel to the graphene walls for the 0.8 nm slit width and different velocity strain rates. The inset definitions are the same as in Fig.13.

CONCLUSION

A comprehensive Non-Equilibrium Molecular Dynamics (NEMD) campaign is performed to simulate nano-confined water flows between two moving graphene sheets in accordance with the Couette problem for a range of the strain rates and the slit widths. All components of the suggested all-atom NEMD model, such as the number of layers in the graphene sheet and the MD force field details, are selected in accordance with recommendations in the literature and tested to ensure that

sensitivity of the model results to the numerical parameters such as the graphene sheet size and the number of graphene layers is low.

In comparison with the previous experimental and computational studies of graphene/water systems, both the continuum hydrodynamics properties, such as the slip length, the shear viscosity, and the normal stress differences, as well as the atomistic structure details such the lateral radial distribution function, are analysed.

For the large width between the graphene sheets, the model reproduces the behaviour of slip length and viscosity coefficients as reported for similar graphene-water systems in previous experimental and computational studies.

For the sub-nanometer-size confinement, the NEMD simulations reveal that ice structures form in the slit between the graphene sheets. The ice formation promotes the development of "ripples" in the graphene layers whose slow diffusion process agrees with a previous Equilibrium MD investigation. The formation of condensed water state under the strong confinement leads to a notable change in mechanical properties of water such as breaking of the rotational symmetry in the plane normal to the applied shear. The simulations reveal that the slip length decreases and the shear viscosity coefficient is amplified when the slit width between the graphene layers decreases. Besides, for the sub-nanometer confinement case, it is shown that the shear viscosity is further amplified when the velocity strain decreases. Then, by extrapolation of the NEMD results to the 1 kHz range of velocity strain rates used in the experiments, it is shown that the shear viscosity of water under the sub-nanometer size confinement is a factor of 4-5 larger in comparison with the bulk value. Notably, this amplification is not as drastic as predicted from some previous Equilibrium Molecular Dynamics (EMD) simulations and also from Atomic Force Microscope (AFM) experiments. It is further argued that the validity of the Green-Kubo relation for viscosity

calculation in nano-confined liquids is debatable while the indirect methods of viscosity calculation used in AFM is also prone to error because of the non-parallel effects between the AFM tip surface and the substrate surface which makes the accurate resolution of tangential and normal force components difficult.

The change of the material properties of water under the sub-nanometer confinement is attributed to the formation of a long-range order in the lateral radial distribution function of water atoms as typical of the crystal-like behaviour. The response of the condensed-state-like water to applied velocity strain rates is also notably different in comparison with that of the liquid-like water at room temperature. While the liquid state-like water shows a shear thinning effect at higher strain rates, which leads to some smearing of the lateral radial distribution of water atoms, the water structure in the condensed-like state is virtually independent on the applied strain rate. In this condensed-like state, water behaves like a frozen slab sliding between the two moving graphene walls so that the slip length between the water slab and the graphene layers increases with the strain rate increase. It can also be speculated that the effect of graphene layer rheology due to the flexibility of the graphene/water interface under normal stresses is competing with the effect of shear viscosity increase under the sub-nanometer confinement.

The findings of this study provide a useful reference point for further studies of transport and material properties of water subjected to extreme confinement and shear conditions. These can be further used in the design of nanofluidic devices such as high-permeability membranes as well as for reliable interpretations of the results of AFM experiments.

METHODS

Dipole and quadrupole moments are a key factor for correctly modelling of water transport properties in molecular dynamics simulations[17, 62-65]. In rigid-bond water models, the dipole

moment is generated by placing a partial charge on the oxygen and hydrogen sites. However, using the fixed charge distribution may lead to an underprediction of the dipole moment in water models such as SPC thereby leading to inconsistent shear viscosity, diffusion coefficient and dielectric constant in comparison with experiments[17, 62-63]. In comparison with SPC, SPC/E water model is able to more accurately reproduce water polarisation and dipole moment properties due to a slightly better adjusted atomic partial charge but still gives a too low shear viscosity coefficient in comparison with the experimental data[63]. Another example of the rigid-bond water models is TIP4P that has the best performance among the family of TIP3P/TIP4P/TIP5P models due to its much more elaborate charge distribution and parametrisation[66-68]. Still, TIP4P under-predicts the shear viscosity in comparison with the experiments[63]. A promising method to capture water polarisation effects, which are very important for correct representation of water transport properties, is to introduce flexibility of the intermolecular bonds and angles[18, 62, 64-65]. In particular, SPC/Fw water model is a recent example of the flexible water models which incorporates a changeable dipole moment with respect to the thermodynamic state. The flexible bond model leads to a good agreement with the experimental data for the shear viscosity coefficient[17, 55, 63]. Hence, it is the SPC/Fw water model that has been selected for most MD simulations in this article.

To initialise the NEMD simulation, SPC/Fw water atoms are filled in the slit between the stationary graphene walls. After the initialization step, the top wall moves impulsively in accordance with the Couette flow conditions for a range of strain rates from 1.32×10^{10} s^{-1} to 23.68×10^{10} s^{-1}. The range of considered strain rates is sufficiently large to investigate the effect of shear on material properties of water under confinement without producing notable numerical artefacts such noise or spurious heating effects contaminating the NEMD results.

In order to model interactions between the carbon atoms in graphene layers, the so-called optimised Tersoff potential is used. This is an optimized version of Tersoff 1989[69-70] which has been used associated with the modified Lennard-Jones (L-J) potential based on ε_{cc} =0.298 kJ/mol and $\sigma_{cc} = 3.14$Å to simulate water confined between graphene layers[33]. The carbon-water interactions are also modelled by the L-J potential where ε_{co} =0.392 kJ/mol and σ_{co} =3.19Å as recommended in previous publications[71]. The L-J cutoff distance is 1.5 nm and the Coulombic interaction is modelled by the PPPM algorithm with the target accuracy of 10^{-6}.

As a side remark, it can be noted that other choices for the molecular dynamics potentials of the same family include Tersoff 1990[72], Tersoff 1994[73] and the optimized Tersoff[69]. Previous studies[74] found that the Tersoff 1989 is able to produce the correct graphene structure e.g. carbon-carbon distance in graphene whereas the Tersoff 1990 and Tersoff 1994 models cannot. All these models can well produce the Young's moduli. In comparison with its modified version[69] used in the present study, Tersoff 1989 cannot accurately reproduce the phonon dispersions of graphene, which is used to characterize anharmonic and harmonic interactions between atoms. The latter is important since the harmonic and non-harmonic interactions determine the bending deformation ("ripples") of graphene layers[75-77]. Most notably, the optimized Tersoff potential has already been validated in application to water-graphene simulations and resulted in good a prediction of the hydrodynamic properties[33]. In order to verify the recommendations in the literature, in addition to the optimized Tersoff model, we also implemented and tested a few other models mentioned above. Notably, none of them gives a stable result for the nano-confined graphene/water system once the slit width reduces to 1 nm or less.

Parameters of the graphene/water model such as the number of layers in the graphene walls and the slit width are varied in order to analyse their effect on the transport and structure water

properties. The number of graphene layers from 2 to 6 and several slit widths in the range from 0.8 nm to 3.8 nm and 0.2 nm step are considered. The number of water molecules in the slit is adjusted to reach the targeted water density of 1 g/cm^3. The effective volume occupied by water atoms in the slit is calculated by excluding the volume occupied by graphene whose Van der Waals force radius is 0.17 nm. The graphene layers have a rectangular shape of 3.5 nm times 3.6 nm, or 8 nm times 8 nm for the larger domain, that matches dimensions of the computational box in the *x*- and the *y*-direction, respectively. Periodic boundary conditions are applied in all directions except for *z* where the domain is confined by graphene layers.

Prior to starting the Couette flow, an initial minimisation and equilibration of the MD model is performed. During the equilibration stage, all internal graphene layers and water atoms are put in contact with the Langevin thermostat with the time constant of 0.1 ps to reach the target temperature of 300 K. The equilibration calculation time is 1 ns and the time step of the MD solution is 1 fs. The time step of the following NEMD simulation is 0.1 fs.

The use of thermostat for nano-confined water atoms is avoided since dissipation of energy in the steady Couette case should be achieved through wall boundaries rather than through the water volume that can lead to unphysical results[78-81]. After completing the equilibration step, the main NEMD simulations are performed where the thermostat is activated only in the flexible graphene layers. Both the equilibration and the subsequent NEMD simulations are based on the NVT ensemble. The run time of NEMD simulations over which the statistical averaging of the solution is performed depends on the strain rate and varies from 10 to 90 ns.

To calculate the slip length and the shear viscosity coefficient, the velocity profile across the slit is calculated from the NEMD simulation. In this process, the entire water volume is divided into bins in the *z*-direction. For each bin, the stream-wise velocity of all water atoms is volume and

time averaged, assuming the statistical homogeneity of the atom distribution in the entire (x-y) plane and the corresponding stationarity in time. The obtained area-averaged velocity profile, $u_x(z)$ and its slope $\frac{du_x}{dz}$ are computed from the discrete bin values using the least square method.

The dynamic shear viscosity coefficient, μ is computed assuming the Newtonian stress-strain relationship for water[82-83]:

$$\mu = \frac{F_{x,top}}{A_{xy}} / \frac{\partial u_x}{\partial z} \quad (1)$$

Here A_{xy} and $F_{x,top}$ are the area of the graphene sheet in (*x*-*y*) plane and the integral viscous shear force applied to the graphene sheet in the flow direction, respectively. The shear force is calculated from results of the NEMD simulation by summing up all non-bond forces, which are exerted on the graphene sheet due to the water/graphene interaction in the flow direction. It can be noted that the error of the viscosity coefficient calculation is mainly due to that of computing the velocity gradient (Supporting Information II, Part 5).

To analyse the water structure properties in the slit confined in the *z*-direction, the lateral radial distribution function (LRDF) is calculated in (*x*-*y*) plane following the definition suggested in the literature[24].

$$g_{xy}(r) = \frac{1}{\rho^2 V} \sum_{i \neq j} \delta(r - r_{ij}) \left[\theta\left(|z_i - z_j| + \frac{\delta z}{2} \right) - \theta\left(|z_i - z_j| - \frac{\delta z}{2} \right) \right] \quad (2)$$

Here ρ,V,r_{ij} and z_i are the number density, volume of the water, pairwise distance in (*x*-*y)* plane and atom coordinates in *z* direction, respectively. $\delta(x)$ and $\theta(x)$ are Dirac delta-function and Heaviside function. Following recommendations in the literature[24], the lateral width of the distribution is set to δz=0.1 nm.

In addition to the main NVT simulation runs, a separate series of simulations is performed where a boundary-controlled barostat is applied to control the pressure of the graphene-water system[49-

[50]. The barostat implementation is based on fixing the outermost graphene layers only in the *x* and *y* direction while allowing the *z*-coordinates of the layers to be adjusted dynamically in the simulation. The vertical adjustment is performed so that the target 1bar pressure is maintained in the system at all times. It has become apparent that the lack of control of the effective width of the graphene slit that occurs during the NPT simulations interferes with the mechanism of liquid-state water to solid-state-like water transition for the sub-nanometer slit width (Supporting information II, Part 1-4). It has been further confirmed that the NPT simulations with applying the barostat to either the top layer or both the top and the bottom graphene layers lead to similar incorrect results. In consistence with the previous nano-confined water investigations[30], this has proven that the liqud-to-solid transition process is very sensitive to how commensurate the width of the graphene slit is with respect to the molecular size of water and one should use NVT simulations for this problem.

ASSOCIATED CONTENT

Supporting Information

Supporting Information I: Evaluation of the NPT model for the nano-confined water simulations and the NEMD simulation error analysis.

Supporting Information II: Computation of the shear viscosity coefficient, the wall forces, and the pressure in the system

Supporting Information III: Evaluation of the Green-Kubo method for computation of the nano-confined water viscosity and discussion of the viscosity effects in the AFM experiment

Supporting Information IV: A video of equilibrium simulation of 0.8 nm gap for 30 ns, the view along X axis.

Supporting Information V: A video of equilibrium simulation of 0.8 nm gap for 30 ns, the view along Y axis.

Supporting Information VI: Independence of the water/graphene system properties of the local features of the graphene layers.

AUTHOR INFORMATION

Corresponding Author

Email: f.li@qmul.ac.uk

Notes

The authors declare no competing financial interest.

ACKNOWLEDGMENT

The work of F.L. was supported by the China Scholarship Council (CSC). I.A.K. gratefully acknowledges the funding under the Marie Skłodowska-Curie Individual Fellowship Grant No. H2020-MSCA-IF-2015-700276 (HIPPOGRIFFE). This research utilised Queen Mary's Apocrita HPC facility, supported by QMUL Research-IT[84].

REFERENCES

1. Sparreboom, W.; van den Berg, A.; Eijkel, J. C. T., Principles and applications of nanofluidic transport. *Nature Nanotechnology* **2009,** *4*, 713.
2. Craighead, H. G., Nanoelectromechanical Systems. *Science* **2000,** *290* (5496), 1532.
3. Cheng, L.-J.; Guo, L. J., Ionic Current Rectification, Breakdown, and Switching in Heterogeneous Oxide Nanofluidic Devices. *ACS Nano* **2009,** *3* (3), 575-584.
4. Raidongia, K.; Huang, J., Nanofluidic Ion Transport through Reconstructed Layered Materials. *Journal of the American Chemical Society* **2012,** *134* (40), 16528-16531.
5. Majumder, M.; Chopra, N.; Andrews, R.; Hinds, B. J., Enhanced flow in carbon nanotubes. *Nature* **2005,** *438*, 44.
6. Holt, J. K.; Park, H. G.; Wang, Y.; Stadermann, M.; Artyukhin, A. B.; Grigoropoulos, C. P.; Noy, A.; Bakajin, O., Fast Mass Transport Through Sub-2-Nanometer Carbon Nanotubes. *Science* **2006,** *312* (5776), 1034.
7. Nair, R. R.; Wu, H. A.; Jayaram, P. N.; Grigorieva, I. V.; Geim, A. K., Unimpeded Permeation of Water Through

Helium-Leak–Tight Graphene-Based Membranes. *Science* **2012,** *335* (6067), 442.
8. Kannam, S. K.; Todd, B.; Hansen, J. S.; Daivis, P. J., How fast does water flow in carbon nanotubes? *The Journal of Chemical Physics* **2013,** *138* (9), 094701.
9. Falk, K.; Sedlmeier, F.; Joly, L.; Netz, R. R.; Bocquet, L., Molecular Origin of Fast Water Transport in Carbon Nanotube Membranes: Superlubricity versus Curvature Dependent Friction. *Nano Letters* **2010,** *10* (10), 4067-4073.
10. Vinogradova, O. I., Slippage of water over hydrophobic surfaces. *International Journal of Mineral Processing* **1999,** *56* (1), 31-60.
11. Vinogradova, O. I.; Belyaev, A. V., Wetting, roughness and flow boundary conditions. *Journal of Physics: Condensed Matter* **2011,** *23* (18), 184104.
12. Ortiz-Young, D.; Chiu, H.-C.; Kim, S.; Voïtchovsky, K.; Riedo, E., The interplay between apparent viscosity and wettability in nanoconfined water. *Nature communications* **2013,** *4*.
13. Li, D.; Wang, Y.; Pan, Y.; Zhao, X., Measurements of slip length for flows over graphite surface with gas domains. *Applied Physics Letters* **2016,** *109* (15), 151602.
14. Maali, A.; Cohen-Bouhacina, T.; Kellay, H., Measurement of the slip length of water flow on graphite surface. *Applied Physics Letters* **2008,** *92* (5), 053101.
15. Abascal, J. L. F.; Vega, C., Dipole-Quadrupole Force Ratios Determine the Ability of Potential Models to Describe the Phase Diagram of Water. *Physical Review Letters* **2007,** *98* (23), 237801.
16. Abascal, J. L. F.; Vega, C., The Water Forcefield: Importance of Dipolar and Quadrupolar Interactions. *The Journal of Physical Chemistry C* **2007,** *111* (43), 15811-15822.
17. Medina, J. S.; Prosmiti, R.; Villarreal, P.; Delgado-Barrio, G.; Winter, G.; González, B.; Alemán, J. V.; Collado, C., Molecular dynamics simulations of rigid and flexible water models: Temperature dependence of viscosity. *Chemical Physics* **2011,** *388* (1–3), 9-18.
18. Raabe, G.; Todd, B. D.; Sadus, R. J., Molecular simulation of the shear viscosity and the self-diffusion coefficient of mercury along the vapor-liquid coexistence curve. *The Journal of Chemical Physics* **2005,** *123* (3), 034511.
19. Li, T.-D.; Chiu, H.-C.; Ortiz-Young, D.; Riedo, E., Nanorheology by atomic force microscopy. *Review of Scientific Instruments* **2014,** *85* (12), 123707.
20. Li, T.-D.; Gao, J.; Szoszkiewicz, R.; Landman, U.; Riedo, E., Structured and viscous water in subnanometer gaps. *Physical Review B* **2007,** *75* (11), 115415.
21. Neek-Amal, M.; Peeters, F. M.; Grigorieva, I. V.; Geim, A. K., Commensurability Effects in Viscosity of Nanoconfined Water. *ACS Nano* **2016,** *10* (3), 3685-3692.
22. Algara-Siller, G.; Lehtinen, O.; Wang, F. C.; Nair, R. R.; Kaiser, U.; Wu, H. A.; Geim, A. K.; Grigorieva, I. V., Square ice in graphene nanocapillaries. *Nature* **2015,** *519*, 443.
23. Han, S.; Choi, M. Y.; Kumar, P.; Stanley, H. E., Phase transitions in confined water nanofilms. *Nature Physics* **2010,** *6*, 685.
24. Kumar, P.; Buldyrev, S. V.; Starr, F. W.; Giovambattista, N.; Stanley, H. E., Thermodynamics, structure, and dynamics of water confined between hydrophobic plates. *Physical Review E* **2005,** *72* (5), 051503.
25. Agrawal, K. V.; Shimizu, S.; Drahushuk, L. W.; Kilcoyne, D.; Strano, M. S., Observation of extreme phase transition temperatures of water confined inside isolated carbon nanotubes. *Nature Nanotechnology* **2016,** *12*, 267.
26. Qiu, H.; Zeng, X. C.; Guo, W., Water in Inhomogeneous Nanoconfinement: Coexistence of Multilayered Liquid and Transition to Ice Nanoribbons. *ACS Nano* **2015,** *9* (10), 9877-9884.
27. Zhu, W.; Zhu, Y.; Wang, L.; Zhu, Q.; Zhao, W.-H.; Zhu, C.; Bai, J.; Yang, J.; Yuan, L.-F.; Wu, H.; Zeng, X. C., Water Confined in Nanocapillaries: Two-Dimensional Bilayer Squarelike Ice and Associated Solid–Liquid–Solid Transition. *The Journal of Physical Chemistry C* **2018,** *122* (12), 6704-6712.
28. Takaiwa, D.; Hatano, I.; Koga, K.; Tanaka, H., Phase diagram of water in carbon nanotubes. *Proceedings of the National Academy of Sciences* **2008,** *105* (1), 39-43.
29. Jinesh, K. B.; Frenken, J. W. M., Experimental Evidence for Ice Formation at Room Temperature. *Physical Review Letters* **2008,** *101* (3), 036101.
30. Ruiz Pestana, L.; Felberg, L. E.; Head-Gordon, T., Coexistence of Multilayered Phases of Confined Water: The Importance of Flexible Confining Surfaces. *ACS Nano* **2018,** *12* (1), 448-454.
31. Yoshida, H.; Kaiser, V.; Rotenberg, B.; Bocquet, L., Dripplons as localized and superfast ripples of water confined between graphene sheets. *Nature Communications* **2018,** *9* (1), 1496.
32. Petravic, J.; Harrowell, P., On the equilibrium calculation of the friction coefficient for liquid slip against a

wall. *The Journal of chemical physics* **2007,** *127* (17), 174706.
33. Ramos-Alvarado, B.; Kumar, S.; Peterson, G. P., Hydrodynamic slip length as a surface property. *Physical Review E* **2016,** *93* (2), 023101.
34. Barati Farimani, A.; Aluru, N. R., Existence of Multiple Phases of Water at Nanotube Interfaces. *The Journal of Physical Chemistry C* **2016,** *120* (41), 23763-23771.
35. Christian, M. R.; Andrea, G.; Matthias, K., Viscosity of a sheared correlated (near-critical) model fluid in confinement. *Journal of Physics: Condensed Matter* **2017,** *29* (33), 335101.
36. Hyżorek, K.; Tretiakov, K. V., Thermal conductivity of liquid argon in nanochannels from molecular dynamics simulations. *The Journal of Chemical Physics* **2016,** *144* (19), 194507.
37. Kubo, R., Statistical-Mechanical Theory of Irreversible Processes. I. General Theory and Simple Applications to Magnetic and Conduction Problems. *Journal of the Physical Society of Japan* **1957,** *12* (6), 570-586.
38. Petravic, J.; Harrowell, P., Linear response theory for thermal conductivity and viscosity in terms of boundary fluctuations. *Physical Review E* **2005,** *71* (6), 061201.
39. Petravic, J.; Harrowell, P., An equilibrium calculation of the thermal transport coefficients between two planes of arbitrary separation in a condensed phase. *The Journal of Chemical Physics* **2006,** *124* (4), 044512.
40. Rudyak, V. Y.; Belkin, A. A., Fluid viscosity under confined conditions. *Doklady Physics* **2014,** *59* (12), 604-606.
41. Ye, H.; Zhang, H.; Zhang, Z.; Zheng, Y., Size and temperature effects on the viscosity of water inside carbon nanotubes. *Nanoscale Research Letters* **2011,** *6* (1), 87-87.
42. Babu, J. S.; Sathian, S. P., The role of activation energy and reduced viscosity on the enhancement of water flow through carbon nanotubes. *The Journal of chemical physics* **2011,** *134* (19), 194509.
43. Shaat, M., Viscosity of Water Interfaces with Hydrophobic Nanopores: Application to Water Flow in Carbon Nanotubes. *Langmuir* **2017,** *33* (44), 12814-12819.
44. Chen, X.; Cao, G.; Han, A.; Punyamurtula, V. K.; Liu, L.; Culligan, P. J.; Kim, T.; Qiao, Y., Nanoscale Fluid Transport: Size and Rate Effects. *Nano Letters* **2008,** *8* (9), 2988-2992.
45. Wagemann, E.; Oyarzua, E.; Walther, J. H.; Zambrano, H. A., Slip divergence of water flow in graphene nanochannels: the role of chirality. *Physical Chemistry Chemical Physics* **2017**.
46. Kumar Kannam, S.; Todd, B. D.; Hansen, J. S.; Daivis, P. J., Slip length of water on graphene: Limitations of non-equilibrium molecular dynamics simulations. *The Journal of Chemical Physics* **2012,** *136* (2), 024705.
47. Hu, H.; Bao, L.; Priezjev, N. V.; Luo, K., Identifying two regimes of slip of simple fluids over smooth surfaces with weak and strong wall-fluid interaction energies. *The Journal of chemical physics* **2017,** *146* (3), 034701.
48. Ramos-Alvarado, B.; Kumar, S.; Peterson, G., Hydrodynamic slip in silicon nanochannels. *Physical Review E* **2016,** *93* (3), 033117.
49. Ewen, J. P.; Gattinoni, C.; Morgan, N.; Spikes, H. A.; Dini, D., Nonequilibrium Molecular Dynamics Simulations of Organic Friction Modifiers Adsorbed on Iron Oxide Surfaces. *Langmuir* **2016,** *32* (18), 4450-4463.
50. Gattinoni, C.; Maćkowiak, S.; Heyes, D. M.; Brańka, A. C.; Dini, D., Boundary-controlled barostats for slab geometries in molecular dynamics simulations. *Physical Review E* **2014,** *90* (4), 043302.
51. Schmatko, T.; Hervet, H.; Leger, L., Friction and Slip at Simple Fluid-Solid Interfaces: The Roles of the Molecular Shape and the Solid-Liquid Interaction. *Physical Review Letters* **2005,** *94* (24), 244501.
52. Martini, A.; Hsu, H.-Y.; Patankar, N. A.; Lichter, S., Slip at High Shear Rates. *Physical Review Letters* **2008,** *100* (20), 206001.
53. Sendner, C.; Horinek, D.; Bocquet, L.; Netz, R. R., Interfacial Water at Hydrophobic and Hydrophilic Surfaces: Slip, Viscosity, and Diffusion. *Langmuir* **2009,** *25* (18), 10768-10781.
54. Cho, J.-H. J.; Law, B. M.; Rieutord, F., Dipole-Dependent Slip of Newtonian Liquids at Smooth Solid Hydrophobic Surfaces. *Physical Review Letters* **2004,** *92* (16), 166102.
55. Wu, Y.; Tepper, H. L.; Voth, G. A., Flexible simple point-charge water model with improved liquid-state properties. *The Journal of Chemical Physics* **2006,** *124* (2), 024503.
56. Kapoor, K.; Patil, S., Viscoelasticity and shear thinning of nanoconfined water. *Physical Review E* **2014,** *89* (1), 013004.
57. Khan, S. H.; Matei, G.; Patil, S.; Hoffmann, P. M., Dynamic solidification in nanoconfined water films. *Physical review letters* **2010,** *105* (10), 106101.
58. Mosaddeghi, H.; Alavi, S.; Kowsari, M. H.; Najafi, B., Simulations of structural and dynamic anisotropy in nano-confined water between parallel graphite plates. *The Journal of Chemical Physics* **2012,** *137* (18), 184703.
59. Li, T.-D.; Riedo, E., Nonlinear Viscoelastic Dynamics of Nanoconfined Wetting Liquids. *Physical Review Letters*

2008, *100* (10), 106102.
60. Foss, D. R.; Brady, J. F., Structure, diffusion and rheology of Brownian suspensions by Stokesian Dynamics simulation. *Journal of Fluid Mechanics* **2000,** *407*, 167-200.
61. Subramaniyan, A. K.; Sun, C. T., Continuum interpretation of virial stress in molecular simulations. *International Journal of Solids and Structures* **2008,** *45* (14), 4340-4346.
62. Raabe, G.; Sadus, R. J., Molecular dynamics simulation of the dielectric constant of water: The effect of bond flexibility. *The Journal of Chemical Physics* **2011,** *134* (23), 234501.
63. Raabe, G.; Sadus, R. J., Molecular dynamics simulation of the effect of bond flexibility on the transport properties of water. *The Journal of Chemical Physics* **2012,** *137* (10), 104512.
64. López-Lemus, J.; Chapela, G. A.; Alejandre, J., Effect of flexibility on surface tension and coexisting densities of water. *The Journal of Chemical Physics* **2008,** *128* (17), 174703.
65. González, M. A.; Abascal, J. L. F., A flexible model for water based on TIP4P/2005. *The Journal of Chemical Physics* **2011,** *135* (22), 224516.
66. Sanz, E.; Vega, C.; Abascal, J. L. F.; MacDowell, L. G., Phase Diagram of Water from Computer Simulation. *Physical Review Letters* **2004,** *92* (25), 255701.
67. Zielkiewicz, J., Structural properties of water: Comparison of the SPC, SPCE, TIP4P, and TIP5P models of water. *The Journal of Chemical Physics* **2005,** *123* (10), 104501.
68. Vega, C.; Abascal, J. L. F.; Conde, M. M.; Aragones, J. L., What ice can teach us about water interactions: a critical comparison of the performance of different water models. *Faraday Discussions* **2009,** *141* (0), 251-276.
69. Lindsay, L.; Broido, D. A., Optimized Tersoff and Brenner empirical potential parameters for lattice dynamics and phonon thermal transport in carbon nanotubes and graphene. *Physical Review B* **2010,** *81* (20), 205441.
70. Tersoff, J., Empirical Interatomic Potential for Carbon, with Applications to Amorphous Carbon. *Physical Review Letters* **1988,** *61* (25), 2879-2882.
71. Werder, T.; Walther, J. H.; Jaffe, R. L.; Halicioglu, T.; Koumoutsakos, P., On the Water−Carbon Interaction for Use in Molecular Dynamics Simulations of Graphite and Carbon Nanotubes. *The Journal of Physical Chemistry B* **2003,** *107* (6), 1345-1352.
72. Tersoff, J., Carbon defects and defect reactions in silicon. *Physical Review Letters* **1990,** *64* (15), 1757-1760.
73. Tersoff, J., Chemical order in amorphous silicon carbide. *Physical Review B* **1994,** *49* (23), 16349-16352.
74. Gayk, F.; Ehrens, J.; Heitmann, T.; Vorndamme, P.; Mrugalla, A.; Schnack, J., Young's moduli of carbon materials investigated by various classical molecular dynamics schemes. *Physica E: Low-dimensional Systems and Nanostructures* **2018,** *99*, 215-219.
75. Gao, W.; Huang, R., Thermomechanics of monolayer graphene: Rippling, thermal expansion and elasticity. *Journal of the Mechanics and Physics of Solids* **2014,** *66*, 42-58.
76. Los, J. H.; Katsnelson, M. I.; Yazyev, O. V.; Zakharchenko, K. V.; Fasolino, A., Scaling properties of flexible membranes from atomistic simulations: Application to graphene. *Physical Review B* **2009,** *80* (12), 121405.
77. Fasolino, A.; Los, J. H.; Katsnelson, M. I., Intrinsic ripples in graphene. *Nature Materials* **2007,** *6* (11), 858-861.
78. Basconi, J. E.; Shirts, M. R., Effects of Temperature Control Algorithms on Transport Properties and Kinetics in Molecular Dynamics Simulations. *Journal of Chemical Theory and Computation* **2013,** *9* (7), 2887-2899.
79. Bernardi, S.; Todd, B. D.; Searles, D. J., Thermostating highly confined fluids. *The Journal of Chemical Physics* **2010,** *132* (24), 244706.
80. Thomas, M.; Corry, B., Thermostat choice significantly influences water flow rates in molecular dynamics studies of carbon nanotubes. *Microfluidics and Nanofluidics* **2015,** *18* (1), 41-47.
81. Yong, X.; Zhang, L. T., Thermostats and thermostat strategies for molecular dynamics simulations of nanofluidics. *Journal of Chemical Physics* **2013,** *138* (8), 084503-084503-10.
82. Boţan, A.; Rotenberg, B.; Marry, V.; Turq, P.; Noetinger, B., Hydrodynamics in Clay Nanopores. *The Journal of Physical Chemistry C* **2011,** *115* (32), 16109-16115.
83. Wang, S.; Javadpour, F.; Feng, Q., Molecular dynamics simulations of oil transport through inorganic nanopores in shale. *Fuel* **2016,** *171*, 74-86.
84. T. King, S. B., and L. Zalewski, Apocrita—High Performance Computing Cluster for Queen Mary *University of London* **2017**.